

Autonomous search of real-life environments combining dynamical system-based path planning and unsupervised learning

Uyiosa Philip Amadasun

Department of Mechanical Engineering
San Diego State University
San Diego, California 92182
philipamadasun1@gmail.com

Patrick McNamee

Department of Mechanical Engineering
San Diego State University
San Diego, California 92182
pmcnamee5123@sdsu.edu

Zahra Nili Ahmadabadi*

Department of Mechanical Engineering
San Diego State University
San Diego, California 92182
zniliyahmadabadi@sdsu.edu

Abstract

In recent years, advancements have been made towards the goal of using chaotic coverage path planners for autonomous search and traversal of spaces with limited environmental cues. However, the state of this field is still in its infancy as there has been little experimental work done. Current experimental work has not developed robust methods to satisfactorily address the immediate set of problems a chaotic coverage path planner needs to overcome in order to scan realistic environments within reasonable coverage times. These immediate problems are as follows: (1) an obstacle avoidance technique which generally maintains the kinematic efficiency of the robot's motion, (2) a means to spread chaotic trajectories across the environment (especially crucial for large and/or complex-shaped environments) that need to be covered, and (3) a real-time coverage calculation technique that is accurate and independent of cell size. This paper aims to progress the field by proposing algorithms that address all of these problems by providing techniques for obstacle avoidance, chaotic trajectory dispersal, and accurate coverage calculation. The algorithms produce generally smooth chaotic trajectories and provide high scanning coverage of environments. These algorithms were created within the ROS framework and make up a newly developed chaotic path planning application. The performance of this application was comparable to that of a conventional optimal path planner. The performance tests were carried out in environments of various sizes, shapes, and obstacle densities, both in real-life and Gazebo simulations.

Keywords: Autonomous robot, Path planning, Unpredictable search, Nonlinear dynamical system.

Availability of data, material, or code: https://gitlab.com/dsim-lab/paper-codes/Autonomous_search_of_real-life_environments

*Corresponding author.

NOMENCLATURE

A	Arnold system's parameter	$n_{TP_{DS-R}}$	A vector containing the last row of TP_{DS-R}
$arnpnt$	Tuple of Arnold system coordinates and accompanied trajectory points	$O_{X,Y}$	Origin of an occupancy-grid map
B	Arnold system's parameter	PDA	Occupancy probability data array
C	Arnold system's parameter	SR	Sensing range
CT	Time for desired coverage rate	SC_a, SC_{r_t}	Scan angle and scan range at t
$Cell_F$	Representation of a cell with occupancy probability value of 0	TF_{MS}	Transformation matrix for map frame to sensing frame
$Cell_O$	Representation of a cell with occupancy probability value of 100	TP_{DS-R}	Temporary matrix of Arnold dynamical system and robot coordinates
$Cell_U$	Representation of a cell with occupancy probability value of -1	TF_{MS_t}	TF_{MS} at a specific time
$Cell_{X,Y}$	Coordinates of a cell in occupancy-grid map	Th_1, Th_2	Cost thresholds
$Cost_{Total}$	Cost of travel to a trajectory point	tp	A set of trajectory points
c_z	Zone's coverage rate	t	Time
DS_{index}	Index for each Arnold dynamical system coordinate	tc	Total coverage rate
d	Distance between the robot and a zone centroid	tp	Trajectory point
dc	Desired coverage rate	tp_{n-1}	The tp at the last iteration
$dist$	Distance between the robot and a cell	tp_{new}	The tp used for replacement
FOV	Field of view of the sensor	v	Robot's velocity
f, g	Cost function parameter	$(X, Y)_M, (X, Y)_S$	Point co-ordinate in the map frame and sensor frame
H, W	Height and width of occupancy grid	$(X, Y)_{RM}, (X, Y)_{SM}$	Robot and sensor pose in the map frame respectively
ind	Index number of cell in probability array	$(X, Y)_{RM_t}, (X, Y)_{SM_t}$	$(X, Y)_{RM}$ and $(X, Y)_{SM}$ at specific time
i, j	Incremental index	$(X, Y)_{zone}$	Centroid of a zone
M_C	Matrix storing coverage status and the zone identification of cells	$x(t), y(t), z(t)$	Coordinates of Arnold system
M_Z	Matrix storing coverage information and the centroid of every zone	zid	Zone identification
n_{iter}	Number of iterations	α	Orientation of a cell from the sensor field of view
ns	Subset of n_{iter}	θ	Mapping variable

1 Introduction

Coverage path planning (CPP) algorithms are primarily developed for the purpose of creating trajectories that enable a robot to visit an area while avoiding any obstacles. Such algorithms have several applications, from use in varied environments such as households (Choi et al., 2017), farm fields (Hameed, 2014), and surveillance and search tasks (Choi et al., 2020; Di Franco and Buttazzo, 2016; Faigl et al., 2011; Grøtli and Johansen, 2012; Hsu et al., 2014; Kapoutsis et al., 2017; Li et al., 2014; Zhu et al., 2019; Bae, 2004a; Bae et al., 2003). One of the relatively recent methods of CPP algorithm development is found in the use of chaotic motion, thus the moniker, chaotic coverage path planning (CCPP). Chaotic motion as a basis for coverage path planning opens some potential advantages over other more established CPP algorithms in the area of surveillance missions. It allows the robot to scan uncertain environments while avoiding obstacles as well as adversarial agents, i.e., unpredictability of the motion enables avoiding attacks. Although the generated trajectories appear random to adversaries, the deterministic nature of these planners provide the possibility of being controlled by the designer to adjust the level of unpredictability and quality of coverage. Studies have used nonlinear dynamical systems (DS) to generate chaotic trajectories (Nakamura and Sekiguchi, 2001; Sridharan et al., 2022; Sridharan and Ahmadabadi, 2020; Volos et al., 2012a; Pimentel-Romero et al., 2017; Nasr et al., 2019; Volos et al., 2013; Tlelo-Cuautle et al., 2014; Volos et al., 2012b; Li et al., 2013; Petavratzis et al., 2021b; Li et al., 2017; Moysis et al., 2021; Petavratzis et al., 2020c; Petavratzis et al., 2021a; Majeed, 2020; Sooraska and Klomkarn, 2010; Bae, 2004b; Bae et al., 2003; Bae, 2004a; Bae et al., 2006; Moysis et al., 2020a; Nwachima and Pérez-Cruz, 2021; Petavratzis et al., 2020a; Jansri et al., 2004; Zhang, 2018; Chu et al., 2022; Fallahi and Leung, 2010). Nakamura and Sekiguchi (Nakamura and Sekiguchi, 2001) showed that while algorithms like random walk generate unpredictable trajectories, the density of said trajectories are less uniform than that of chaotic model. This is because the random walk algorithm resists continuity in the robots motion where the chaotic model does not. To build off this earlier work, other studies introduced the chaos manipulation techniques including random number generators (Pimentel-Romero et al., 2017), as well as arccosine and arcsine transformations (Li et al., 2013) to improve dispersal of trajectory points across an environment map. While these methods might have indirectly helped to decrease the coverage time to some extent, they mostly focused on improving the coverage rate rather than the coverage time. Our work in Sridharan et al., 2022 focused on increasing the efficiency of the chaotic path planning approaches by specifically controlling the chaotic trajectories to directly reduce the coverage time. These works proposed various chaos control techniques to make the planner adaptable and scalable to cover environments varying in size and property within a finite time (Sridharan and Ahmadabadi, 2020). These techniques were successful in significantly reducing the coverage time and bringing it closer to optimal time. While some of these studies have contributed to the subject at hand, the field of CCPP still has much further to go. Most studies discuss techniques which have only been tested in simple environments, such as square shaped simulated environments with little or no variation in obstacle size, shape or density (Sridharan et al., 2022; Li et al., 2013; Petavratzis et al., 2021a; Moysis et al., 2020b; Petavratzis et al., 2020b; Nasr et al., 2019; Pimentel-Romero et al., 2017; Volos et al., 2012a; Volos et al., 2012b; Petavratzis et al., 2021b; Li et al., 2017; Moysis et al., 2021; Petavratzis et al., 2020c; Bae, 2004a; Bae et al., 2003; Bae et al., 2006; Moysis et al., 2020a; Nwachima and Pérez-Cruz, 2021; Petavratzis et al., 2020a; Jansri et al., 2004; Zhang, 2018; Chu et al., 2022; Fallahi and Leung, 2010). Additionally, these simulations were not carried out in specialized simulation software like Gazebo and hardly went beyond MATLAB. As a result, the effectiveness of these techniques in real life testing are currently unknown.

The experimental techniques which have been tested in real life have the same limitations in the context of tested environments. Additionally, these experimental techniques do not tackle the challenges in applying CCPP concepts to the real world. For instance, in previous work (Volos et al., 2013; Majeed, 2020; Tlelo-Cuautle et al., 2014; Sooraska and Klomkarn, 2010), the object avoidance strategy deployed is not robust enough to provide continuous chaotic trajectories which maintain kinematic efficiency as the environments become more complex. In the same fashion, there is no dispersal technique to thoroughly spread chaotic trajectories across the environment. The relevance of a dispersal technique becomes especially apparent in larger environments. As for a coverage calculation technique, the maps of the environments were divided into cells of arbitrary size and coverage was based on the number of cells the trajectory passed through. As this method do not use any sensing information, the coverage calculations might become overestimated or underestimated for the following reasons. (1) Without any sensor input, it is difficult to determine if a cell is fully covered or if the robot only covered part of it. (2) The robot can possibly sense multiple cells at once as it moves across the map. Some of these cells may ultimately not be accounted for due to coverage dictated only by trajectory.

The following summarizes the shortcomings of state-of-the-art experimental techniques and the contributions of this paper to address them:

- (1) There is no previously defined effective technique for obstacle avoidance which maintains kinematic efficiency and smooth trajectories. This paper proposes a new proactive obstacle avoidance technique that utilizes a cost function and a quadtree (Samet, 1988) data structure created from discretized map data to provide quick chaotic path planning capabilities in complex-shaped environments of varying sizes, shapes and obstacle densities.
- (2) There has been no applied means of dispersal of chaotic trajectories in large environments to improve effective coverage, hence reducing coverage time, especially in large and/or complex-shaped environments. This work has developed a map-zoning technique via an unsupervised machine-learning clustering algorithm to disperse chaotic trajectories across the map for more efficient scanning, thus reducing coverage time in large environments.
- (3) Lack of accurate and time-effective methods for real-time implementation of coverage calculation in the field of CCPP raises doubt about the applicability of these planners in real-world environments. This study has developed a real-time computation technique that utilizes discretized map data (via quadtree), sensor data, and storage matrices for fast and accurate coverage rate calculation. Additionally, a multi-threading option is made available for possibly faster computation.

To our knowledge, our approach of using quadtree for fast real-time coverage rate computation (with sensor data) is a novel contribution to the field of coverage path planning. Other papers (Huang et al., 2020; Jan et al., 2019) which discussed the use of the quadtree data structure for CPP application, employed it for the purpose of efficient partitioning of the coverage area into smaller regions (and subregions), thus enabling easier identification of the areas in need of coverage.

These contributions were made through the development of algorithms which communicate with each other via the Robot Operating Software(ROS) framework. The rest of the paper is arranged as follows: Section 2 explains the integration of chaotic systems to develop robot trajectory. Section 3 discusses the path planning and chaos control techniques. Section 4 will discuss results of performance in both simulated Gazebo environments and live tests with varying environments, as well as performance comparison with the well-established boustrophedon path planning algorithm. Section 5 concludes the paper and discusses future work. All algorithms developed in this work are written in the Python language.

2 Integration of chaotic dynamical systems for mobile robot

The chaotic dynamical systems can be in form of continuous (Volos et al., 2012a; Nakamura and Sekiguchi, 2001; Agiza and Yassen, 2001; Li et al., 2016; Lü et al., 2004) or discrete systems (Li et al., 2013; Arrowsmith et al., 1993; Curiac and Volosencu, 2014; Li et al., 2017; Li et al., 2015). This work will use the continuous Arnold system simply because our previous study (Sridharan et al., 2022) showed the potential efficiency and flexibility to adapt and scale to different coverage tasks. The Arnold system (Nakamura and Sekiguchi, 2001) is described by the following equations:

$$\begin{cases} dx(t)/dt = A \sin z(t) + C \cos y(t) \\ dy(t)/dt = B \sin x(t) + C \cos z(t) \\ dz(t)/dt = C \sin y(t) + B \cos x(t) \end{cases} \quad (1)$$

The variables $x(t)$, $y(t)$, and $z(t)$ are the DS coordinates. A , B , and C are the Arnold system parameters. A nonlinear dynamical system becomes chaotic upon gaining these properties: (1) sensitivity to initial conditions (ICs), and (2) topological transitivity. Per our previous work (Sridharan et al., 2022), we use the tuple $(x_0, y_0, z_0) = (0, 1, 0)$ as initial conditions (ICs) for the Arnold system. The Arnold system parameters are chosen to be $A = 0.5$, $B = 0.25$, and $C = 0.25$. The analysis of the parameter space conducted in our previous study (Sridharan et al., 2022) showed

that these values satisfy the properties (1) and (2) for a chaotic system and result in reasonably uniform coverage of the environment when the Arnold system is integrated into the robot's controller.

Fig. 1 shows the 3-D chaos attractor of the Arnold system created using these parameters. The CCPP algorithm maps the DS coordinates into the robot's kinematic equation (Eq. (2)). New states obtained from mapping process are set as trajectory points for the robot to travel to via ROS navigation stack.

$$\begin{cases} dx(t)/dt = v \cos x(t) \\ dy(t)/dt = v \sin x(t) \\ w(t) = d\theta(t)/dt = dx(t)dt \end{cases} \quad (2)$$

where $X(t)$ and $Y(t)$ are the robot's coordinates, v is the robot's velocity, dt is the time step, and $x(t)$ is one of the Arnold system's coordinates mapped into the robot's kinematic relations. The other coordinates of the Arnold system can replace $x(t)$ to perform the mapping, however, the trajectories produced by each coordinate will be different from the others. We will later use this feature in section 3.1.1 to improve coverage. Fig. 2 illustrates the general schematics of a two wheel differential drive mobile robot used in this study. The robot comprises of two active fixed wheels with one passive caster, subject to a non-holonomic constraint.

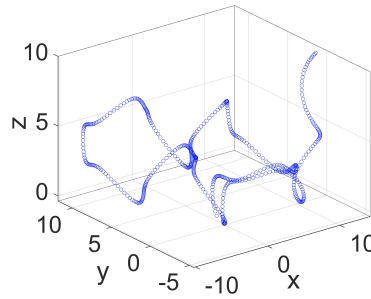


Figure 1: 3-D Chaos attractor for the Arnold system, first published in [add citation] by Springer Nature.

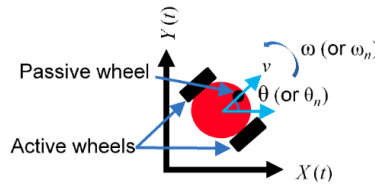


Figure 2: Mobile robot's motion on a plane, first published in [add citation] by Springer Nature.

3 Path planning strategy and chaos control technique

The objective of this work is to tackle the challenges associated with experimental real-time implementation of CCPP. We adapt some of the theoretical chaos control techniques proposed in our previous study (Sridharan et al., 2022) and make them applicable to real-life environments while providing the following contributions. (1) A proactive obstacle avoidance technique which utilizes a cost function and a quadtree data structure created from discretized map data to set trajectories away from obstacles while maintaining general smoothness of trajectory and continuous motion. (2) A map-zoning technique based on an unsupervised machine-learning clustering algorithm which continuously directs the robot to less-visited distant areas of the environment. And (3) a computation technique which is independent of cell

size, but instead based on discretized map data (via quadtree) and sensor data to provide accurate real-time coverage calculation.

$$ind = (Cell_X \times W) + Cell_Y \quad (3)$$

$$\begin{cases} X_M = (Cell_X \times res) + O_X \\ Y_M = (Cell_Y \times res) + O_Y \end{cases} \quad (4)$$

$$\begin{cases} Cell_X = ind \bmod W \\ Cell_Y = \frac{(ind - Cell_X)}{W} \end{cases} \quad (5)$$

$$\begin{cases} Cell_X = \frac{X_M - O_X}{res} \\ Cell_Y = \frac{Y_M - O_Y}{res} \end{cases} \quad (6)$$

In what follows: (1) the algorithms interact with map data information of a 2D occupancy-grid map. (2) Cells refer to the smallest possible segments of the map, while zones represent larger segments. (3) The relevant map data information includes: occupancy probability data array (*PDA*), map resolution (*res*), map height (*H*), map width (*W*), and origin of map ($O_{(X,Y)}$). (4) The *PDA* contains the occupancy probability values of every cell in the occupancy-grid map and the algorithms interact with this information in various ways. Eqs. (3)-(6) are used in several algorithms to convert relevant data field information to useful formats to perform various tasks. Eq. (5) derives the coordinate of a cell in the occupancy-grid map ($Cell_{(X,Y)}$) from its corresponding *PDA* index value (*ind*). Eq. (6) derives the coordinates of a cell ($Cell_{(X,Y)}$) using the $O_{(X,Y)}$ and its map frame coordinate ($(X,Y)_M$). (5) The map of the environment is broken into individual zones before all other algorithms start to run. (6) The quadtree data structure solely contains the $Cell_{(X,Y)}$ positions of every cell which represents free space. The quadtree and the storage matrices (M_Z and M_C) are created (directly or indirectly) using relevant map data information (before the start of any algorithms excluding the unsupervised machine-learning clustering algorithm) for quick queries and zone coverage updates. The quadtree algorithms developed in (Quadtree implementation in Python, 2020) have been adapted for this work. (7) The transformation matrix (TF_{MS}) (created via ROS) transforms point coordinates from the map frame to the sensor frame and is used along with sensor data for coverage calculation. (8) The communications between any algorithms that do not directly invoke each other is performed via the ROS framework. (9) As the robot moves across the map, trajectory points are set as goals by the ROS navigation stack. The navigation stack provides a global path planner based on the Dijkstra algorithm. The DWA and TEB Local planners were tested to see which would be the best. In the final analysis, a DWA local planner is chosen with full awareness of the sub-optimal trajectories it often generates. However, the DWA local planner was chosen for the following reasons: (1) it is less sensitive to the choice of parameters, making it easier to tune and use in different environments. (2) It can handle dynamic obstacles more effectively, as it takes into account the motion of the robot and the motion of other objects in the environment when planning a path. And (3) it is computationally less expensive, making it more suitable for use on robots with limited computational resources. (8) It must be noted that all algorithms are written in the Python language and therefore any indices of any vectors, arrays or matrices discussed starts at 0.

The rest of this section will provide an overview of the CCP process in ROS using the flowchart shown in Fig. 3. As seen in Fig. 3, the occupancy-grid map is created via simultaneous localization and mapping (SLAM). This is the first step. The resulting occupancy grid map is then published as map data. As discussed earlier, part of the map data is the *PDA*. The $(X,Y)_M$ values of all cells that represent free space, are derived from the *ind* values of the aforementioned cells in the *PDA* (using Eqs. (5) and then (4)). These $(X,Y)_M$ values are stored in an array which is fed as part of the input to the clustering algorithm. The clustering algorithm uses this information to divide the environment into zones. The matrix M_Z stores zone information. The storage matrix M_C is created using all the index information from the *PDA* and zone information. M_C keeps track of cell coverage to memory. Then, the chaotic coverage path planning procedure is carried out as thus: The ArnoldTrajectoryPlanner (*ATP*) function (Algorithm 1) uses the Arnold system to generate chaotic trajectories in the map frame continuously until desired coverage (*dc*) is reached. Algorithm 1 utilizes the information provided by the *PDA* to aid obstacle avoidance decision making. Based on this information, Algorithm

1 utilizes Algorithms 2 and 3 to set chaotic trajectories away from obstacles. Algorithm 2 (which Algorithm 1 calls and provides input to) utilizes the quadtree and a cost function comprising of two parameters. Algorithm 2 calculates one of the cost function parameters. Algorithm 2 calls and provides input to Algorithm 3 to calculate and returns the other cost function parameter. Algorithm 2 makes calculations with the cost function via the two aforementioned parameters. Algorithm 2 provides the result of its calculations to Algorithm 1. In this way Algorithm 2 and 3 aid performing the task of obstacle avoidance. Algorithm 5 publishes information about least covered zones as one of its tasks. Algorithm 1 utilizes the information published by Algorithm 5 to spread chaotic trajectories across the map. Algorithms 4, 5 and 6 utilize the ROS sensor_msgs package, ROS tf package, quadtree, M_C and M_Z to continuously calculate coverage until dc is met. Algorithm 4 receives published data from the sensor_msgs and tf package which it feeds as input to Algorithm 5. Algorithm 5 uses this input and information from the quadtree to calculate total coverage with the help of Algorithm 6 (which Algorithm 5 calls and provides input to). Algorithm 6 utilizes and updates information in the storage matrices M_C and M_Z . Algorithm 5 uses the information in M_Z for total coverage calculations. Algorithm 4 continuously calls Algorithm 5, with each call providing algorithm 5 with up to date sensor data and TF_{MS} as inputs to accurately calculate coverage until dc is reached. Once dc is reached, Algorithm 5 publishes messages which prompt Algorithm 4 and 1 to stop. The initial position of the robot in the map frame $((X, Y)_{RM})$ is used as a starting point to generate trajectory points successively. $(X, Y)_{RM}$ is retrieved from the transformation of odometry data using the tf package. Next section starts with discussing the obstacle avoidance technique and explains the interaction between the Algorithms 1, 2, and 3.

Figure 3: Flowchart showing algorithm flow in the ROS1 environment.

The proposed obstacle avoidance technique uses a quadtree and cost function to generate smooth and continuous trajectories around obstacles and provide quick chaotic path planning capabilities in environments varying in size, shape, and obstacle density. Our work creates this quadtree from discretized map data to quickly access occupancy-grid map coordinates representing free space. Conceptually, our technique works as follows: (1) The corresponding *PDA* index value (*ind*) of the trajectory point (*tp*) is calculated and evaluated in the *PDA* to check its probability value. Probability values $\neq 0$ are deemed non-viable. (2) Cells representing free space within some radius (*r*) of a non-viable *tp* are accessed from the quadtree (via querying (Quadtree implementation in Python, 2020)). It should be noted that the *r* value is chosen based on the *res* of the occupancy-grid map. The *res* for all simulations and tests is 0.05 meters per pixel. The chosen *r* of 19 cell lengths value does not reduce computation speed. (3) Each coordinate is evaluated using

a cost function to determine a favorable replacement coordinate. (4) A replacement coordinate is set as the new tp . In scenarios where there are no free cells in the immediate vicinity of a non-viable tp for replacement, additional processes are carried out to generate a viable tp . This case, as well as other special scenarios, will be further discussed in section 3.1.1. Quick access to cell information is critical for fast computation, allowing these steps to take place within a sufficiently short time frame, which is essential for achieving obstacle avoidance without the need to stop motion. General smoothness of the trajectory is maintained as the ROS navigation stack sets the robot to these favorable coordinates. It should be noted that the ROS navigation stack sets the next successive goal once the robot is within some threshold of the current one. This threshold is set to a certain length based on the ROS path messages (nav_msgs/Path.msg, 2023), which provide a list of coordinate points that the robot follows on the path to a goal. In this way, the robot's continuous motion is not hindered.

3.1.1 Algorithm workflow

Algorithm 1 uses the Runge-Kutta fourth-order (RK4) method to propagate Eqs. (1) and (2) and generate the trajectory points. To replace non-viable trajectory points, this work uses two mechanisms a custom cost function proactively set trajectories away from obstacles before they are set as goals (via ROS). In what follows, cells representing free space, obstacle space, and unknown space are designated as $Cell_F$, $Cell_O$, and $Cell_U$, respectively. The time step (Δt) of 2.75 seconds is used for the integration in the RK4 method. This time step ensures the generation of sufficiently smooth trajectories. It is important to note that unknown space represents areas within the map where the state of occupancy is not yet determined. These areas are usually represented by cells in the occupancy-grid map that have not been sensed by the sensor during SLAM. These cells are usually surrounded by cells representing obstacle space. A large bulk of Algorithm 1 is developed into two stages. Each stage will make use of the cost function to judge trajectory points with two thresholds respectively (Th_1 and Th_2). All cost of any replacement tp is judged against Th_1 to improve the odds involved in the search for highly favorable replacement coordinates. Immediately before any viable tp is set as a goal, it is judged against Th_2 .

In this way the tp can be quickly replaced incase it is set too close to obstacle space. This arrangement plays into the Algorithm 1 architecture for the purpose of computational efficiency and generation of smooth trajectories. In the first stage (first for-loop) a set of trajectory points (Tp) are generated using the RK4 method. The procedure is as follows: (1) The RK4 method generates a tp with its accompanied DS coordinates. Both the tp and its DS coordinates are designated as *arnpnt*. Any viable tp is added to set Tp . The *arnpnt* becomes the next row of TP_{DS-R} (and therefore the last row of TP_{DS-R} ($n_{TP_{DS-R}}$)) to then be use for the next iteration. (2) The loop breaks at any iteration where tp is generated outside the boundaries of the occupancy-grid map. This is because there is a higher likelihood that more trajectory points will be successively generated outside the boundaries from this point on. Such a scenario (that is, tp generation outside the boundaries) initiates when the area of an occupancy-grid map that represents the environment is big enough to reach the boundaries of the occupancy-grid map. (3) Upon the the generation of a non-viable tp : (3.1) Algorithm 2 is called to provide a better coordinate to set as new tp (tp_{new}). (3.2) If the cost of tp_{new} is greater than some threshold ($cost > Th_1$), Algorithm 1 changes the current Arnold system coordinate by utilizing deterministic DS_{index} switching. In this way a new tp can be generated with the RK4 method and a different DS_{index} . (3.3) This new tp goes through steps 1 to 3.2. (4) If DS_{index} switching is exhausted, the tp_{new} associated with the least cost is chosen along with the accompanied DS coordinates (to make *arnpnt*) for the next iteration. (5) It is possible that steps 3 to 4 still result in the generation of non-viable tp/tp_{new} . Such a scenario can occur if there are is no $Cell_F$ within r of the non-viable trajectory points examined using Algorithm 2. All unreplaceable non-viable tp are added to set Tp and will be replaced at stage 2. The unreplaceable non-viable tp and associated DS coordinates become *arnpnt*, the procedure in step 1 is followed. Algorithm 1 attempts to replace non-viable tp at stage 1 rather than shutting down the tp generation process (via breaking the loop) for the following reasons. Replacing tp induces a higher likelihood of spreading the chaotic trajectory across the local area around the robot's position, thus increasing the likelihood of covering new cells at a faster rate (ultimately reducing CT).

The second stage successively scrutinizes each $tp \in Tp$ with Algorithm 3 immediately before it is set as a goal (via ROS navigation stack). This provides an additional measurement to replace any non-viable $tp \in Tp$ that could not be replaced in the first stage. The a favorable coordinate is chosen by scrutinizing all $Cell_F$ within r of robot's current position ($(X, Y)_{RM}$) (via Algorithm 2). Any tp with $cost > Th_2$, or tp generated outside of boundaries goes through

Algorithm 1 : $ATP(A, B, C, v)$

```
1:  $|TP_{DS-R}|_{first\ row} \leftarrow [x_0, y_0, z_0, (X, Y)_{RM}]$ 
2: while  $tc < dc$  do
3:   if  $dc$  is reached then
4:     Stop
5:   end if
6:   if  $ns == n_{iter}$  OR last sets of  $ns$  produced many non-viable  $tp$  which could not be "shifted" then
7:     empty  $TP_{DS-R}$ 
8:     Evaluate  $(X, Y)_{zone}$  AND the cells within  $r$  cell lengths of itself with Shift function
9:     Set favorable coordinate from evaluation as a goal
10:     $TP_{DS-R} \leftarrow [x_0, y_0, z_0, (\text{favorable coordinate provided by the } arnpnt \text{ via } Shift \text{ function})]$ 
11:   end if
12:   if  $ns < n_{iter}$  then
13:     if  $ns$  iterations end with the generation of a viable  $tp$  then
14:       empty  $TP_{DS-R}$ 
15:        $TP_{DS-R} \leftarrow n_{TP_{DS-R}}$ 
16:     end if
17:     if  $ns$  iterations end with the generation of a non-viable  $tp$  then
18:       empty  $TP_{DS-R}$ 
19:       Evaluate the cells within  $r$  cell lengths of  $Cell_{X,Y}$  representation  $(X, Y)_{RM}$  with Shift function
20:        $TP_{DS-R} \leftarrow [x_0, y_0, z_0, (\text{favorable coordinate provided by the } arnpnt \text{ via } Shift \text{ function})]$ 
21:     end if
22:   end if
23:    $TP = [ ]$ 
24:    $n_{TP_{DS-R}} \leftarrow TP_{DS-R}$ 
25:   for  $i < ns$  do
26:      $arnpnt \leftarrow Eqs.(1) \text{ and } (2) \text{ with } n_{TP_{DS-R}}, A, B, C, v, dt \text{ and } DS_{index}$ 
27:      $Cell_{X,Y} \leftarrow tp$  (using Eq. (6))
28:      $ind \leftarrow Cell_{X,Y}$  (using Eq. (3))
29:     if  $tp$  is set at a coordinate which does not exist within the occupancy-grid map boundaries then
30:       Add  $tp$  to  $TP$ 
31:        $n_{TP_{DS-R}} \leftarrow arnpnt$ 
32:       Add  $arnpnt$  to  $TP_{DS-R}$ 
33:       Break
34:     end if
35:     if  $tp$  is viable ( $PDA[ind] = 0$ ) then
36:       Repeat Lines 30 -32
37:     end if
38:     if  $tp$  is not viable ( $PDA[ind] \neq 0$ ) then
39:        $[Cost_{Total}, arnpnt] \leftarrow Shift(arnpnt, Cell_{X,Y}, tp_{n-1}, r)$ 
40:       if  $Cost_{Total} \geq Th_1$  then
41:         Repeat Line 26 with different  $DS_{index}$  ( $DS_{index}$  switching)
42:         Repeat Lines 27-37
43:       if  $tp$  is not viable ( $PDA[ind] \neq 0$ ) then
44:         Repeat Lines 39-42
45:         if  $Cost_{Total} \geq threshold$  then
46:           if  $tp$  is not viable ( $PDA[ind] \neq 0$ ); At this point  $DS_{index}$  switching is exhausted then
47:             The  $tp_{new}$  associated with the least  $Cost_{Total}$  is chosen along with the accompanied DS coordinates for the next iteration
48:             Add  $tp_{new}$  to  $TP$ 
49:              $n_{TP_{DS-R}} \leftarrow |Associated\ DS\ coordinates, tp|$ 
50:             Add [Associated DS coordinates,  $tp$ ] to  $TP_{DS-R}$ 
51:           end if
52:         else
53:           Repeat Lines 30 -32
54:         end if
55:       end if
56:     else
57:       Repeat Lines 30 -32
58:     end if
59:   end for
60:   for  $tp \in TP$  do
61:     if  $dc$  is reached then
62:       Stop
63:     end if
64:     if  $Cost_{Total} \geq Th_2$  OR non-viable  $tp$  then
65:       Replace the  $tp$  using Shift function just as in line 19.
66:     end if
67:     Set  $tp$  as goal
68:   end for
69: end while
```

the same process as a non-viable tp . The replacement in the second stage is done in this way as it has proved to aid in generation of smooth trajectories. There is a reason for the separation of Algorithm 1 into two stages. In trying to balance the generation of trajectory points with the following outcomes: (1) Successful obstacle avoidance, (2) spread of chaotic trajectories, and (3) generally smooth and continuous motion, the processes of Algorithm 1 must be broken down in a computationally efficient manner. Trying to handle all these processes in one stage would be detrimental to this balance, specifically the third outcome.

In the application of a large number of iterations (n_{iter}), the n_{iter} is broken down into subset ns to iterate at a time so as to not hinder computation speed. It is therefore pertinent to instigate some sort of continuation between all $ns \in n_{iter}$. In order to do so, Algorithm 1 carries out the following: (1) For all $ns \in n_{iter}$ of trajectory points that ends with the generation of either a tp set outside the boundaries, or an unreplaceable non-viable tp : Algorithm 1 calls Algorithm 2 to find a favorable point coordinate around the $(X, Y)_{RM}$ as part of new IC. DS coordinates (x_0, y_0, z_0) and point coordinate associated with this IC are set as first entry to TP_{DS-R} for the next set of iterations. (2) For all $ns \in n_{iter}$ of trajectory points that ends with viable tp : the last set of DS coordinates and tp ($n_{TP_{DS-R}}$) are set as new IC which becomes the first entry to TP_{DS-R} for the next set of iterations. Section 3.2 discusses the cost function in detail.

Algorithm 2 : *Shift*($arnpnt, tp_{n-1}$)

```

1: Query every  $Cell_F$  within  $r$  of  $tp$ 
2: if no  $Cell_F$  within  $r$  then
3:   return no  $Cell_F$  within  $r$ 
4: end if
5: for  $Cell_F \in Query$  do
6:    $(X, Y)_M \leftarrow Cell_{(X, Y)}$  using Eq. (4)
7:    $g \leftarrow CostCalculator(Cell_{(X, Y)})$ 
8:   if First stage then
9:      $f$  is distance between  $tp_{n-1}$  and  $(X, Y)_M$ 
10:  else
11:     $f = 0$ 
12:  end if
13:   $Cost_{Total} \leftarrow$  Eq. (7)
14: end for
15:  $tp_{new} \leftarrow (X, Y)_M$  associated with lowest  $Cost_{Total}$ 
16:  $tp \leftarrow tp_{new}$ 
17: return  $|Cost_{Total}, arnpnt|$ 

```

Algorithm 3 : *CostCalculator*($Cell_{(X, Y)}$)

```

1:  $Cells_B = []$ 
2: for  $i = 0; i \leq l; i = i + 1$  do
3:   get  $Cell_{X-i}$  and  $Cell_{X+i}$ 
4:   for  $j = 0; j \leq l; j = j + 1$  do
5:     get  $Cell_{Y-j}$  and  $Cell_{Y+j}$ 
6:     append all encompassing  $Cell_{X, Y}$  coordinates to  $Cells_B$ 
7:   end for
8: end for
9: return  $g \leftarrow$  Average of probability values of all  $Cell_{X, Y} \in Cells_B$ .

```

3.1.2 Custom cost functions

Algorithms 2 and 3 use a cost function (Eq. (7)) to help Algorithm 1 generate trajectory points away from obstacles. Algorithms 2 and 3 calculate cost function parameters f and g respectively. In Eq. (7), the parameter f is the distance between the generated tp in the last iteration (tp_{n-1}) and the point coordinate $((X, Y)_M)$ of the $Cell_F$ being evaluated. The *Shift* function (Algorithm 2) calculates f . The variable g is the cost of travelling to said $(X, Y)_M$. The parameter

g is the average of assigned values of the coordinates within range l (6 cell lengths in Algorithm 3) of the $Cell_F$ being evaluated. The assigned values are as follows: (1) Any coordinate position which matches a cell position is assigned the absolute value of the occupancy probability of that cell. The probability values of $Cell_O$, $Cell_U$ and $Cell_F$ are 100, -1, and 0 respectively. (2) Any coordinate position which does not match a cell location, in other words, is not within the occupancy-grid boundaries is assigned a value of 500. Such as position is assigned the highest cost so as to set trajectories away from the occupancy-grid map boundaries. Additionally, this likelihood of generating trajectory points outside the boundaries is reduced. The values of every coordinate position used in averaging is gathered in the temporary array $Cells_B$. The tp_{new} is derived from the cell associated with the lowest $Cost_{Total}$. In the second stage of Algorithm 1, the *Shift* function sets f as 0. Fig. 4 shows an example of how this works in practice. In this example, r and l are 2 and 1 cell lengths, respectively. Algorithm 2 successively evaluates each $Cell_F \in Query$ (all within r cell lengths of non-viable tp (red)) with the aid of Algorithm 3 and selects the one with the lowest cost. If multiple $Cell_F \in Query$ share the lowest cost value calculated, the first $Cell_F \in Query$ to be evaluated at that cost value is chosen for tp_{new} . Section 3.2 will discuss Algorithms 4, 5, and 6 in greater detail regarding their role after the map of the environment has been broken down into individual zones.

$$Cost_{Total} = f + g \quad (7)$$

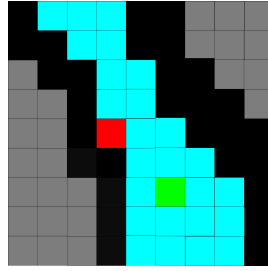


Figure 4: Process for replacement of a non-viable tp : r and l are 2 and 1 respectively. Of all $Cell_F \in Query$ which are within r cell lengths of non-viable tp (red), the $Cell_{(X,Y)}$ of $Cell_F$ which is highlighted as a green cell has the lowest cost. It is the only $Cell_F \in Query$ completely surrounded by other $Cell_F$ within l cell lengths of itself. Therefore, the tp_{new} is derived from the green cell.

3.2 Map-zoning Technique

This technique uses an unsupervised machine-learning clustering algorithm to break the map into individual zones, dispersing chaotic trajectories across the map for more effective scanning and reducing coverage time in large and/or complex environments. The clustering process groups the $(X, Y)_M$ coordinates of all $Cell_F$ into different zones, which takes place before the start of the coverage. The clustering algorithms were obtained from the scikit-learn Python library. Several tests led to the selection of two agglomerative clustering algorithms, ward and k-means, which worked best for grouping cells in a sensible manner. K-means was ultimately chosen because it could create clusters for larger maps, while the ward algorithm ran into memory errors for those maps. The parameters of the k-means algorithm were set to enable sensible centroid assignment and cluster formation (see Figs. 5(a)-(c)) within a reasonable computation time. The centroid of a cluster represents the midpoint $((X, Y)_{zone})$ of the zone. Each zone's midpoint and coverage are stored in memory so that the coverage is continuously updated as the robot traverses the map, and the $(X, Y)_{zone}$ of the least covered zone can be published by Algorithm 5. If there are multiple zones with the least coverage, the $(X, Y)_{zone}$ of the closest distance d to the robot's current position is published. Matrix M_Z stores information about the individual zones, with columns containing the following data from left to right: X_{zone} , Y_{zone} , the number of $Cell_F$ in each zone, the number of $Cell_F$ covered in a zone, and the zone's coverage rate (c_z).

Algorithm 5 utilizes M_Z to analyze which zones are least covered. The coverage of every zone is updated by the *Worker* function (Algorithm 6), which is invoked by Algorithm 5. Algorithm 1 receives $(X, Y)_{zone}$ messages to spread the chaotic trajectories. To do so, Algorithm 1 sets the goal as $(X, Y)_{zone}$. Upon the robot reaching the immediate vicinity to the goal, a new chaotic trajectory is generated with (x_o, y_o, z_o) and $(X, Y)_{zone}$ as the IC. Algorithm 1 carries out this procedure after every n_{iter} or if successive sets of ns contain a high number of non-viable tp , which could not be

replaced even at the second stage. All parameters used by the k-means clustering algorithm are set to values that enable relatively quick and sensible clustering. Examples in Figs. 5(a)-(c) show the map-zoning technique used on maps of varying shapes, sizes, and obstacle densities, with the zones represented by different colors and centroids shown with red dots. In environments with medium to high obstacle densities, a centroid may sometimes be set close to obstacles. In such cases, Algorithm 1 calls Algorithm 2 to evaluate the cost of the centroid all $Cell_F$ within r cell lengths of it. If the centroid shares the lowest cost with any other $Cell_F \in Query$, the shift function chooses the centroid as part of its output. If centroid is not associated with least cost, the first $Cell_F \in Query$ to be evaluated at least cost is chosen at part of output. The associated $(X, Y)_M$ of the chosen cell is set as a goal and used for IC. Section 3.3 will further discuss the role of Algorithms 4, 5 and 6 after zones are created.

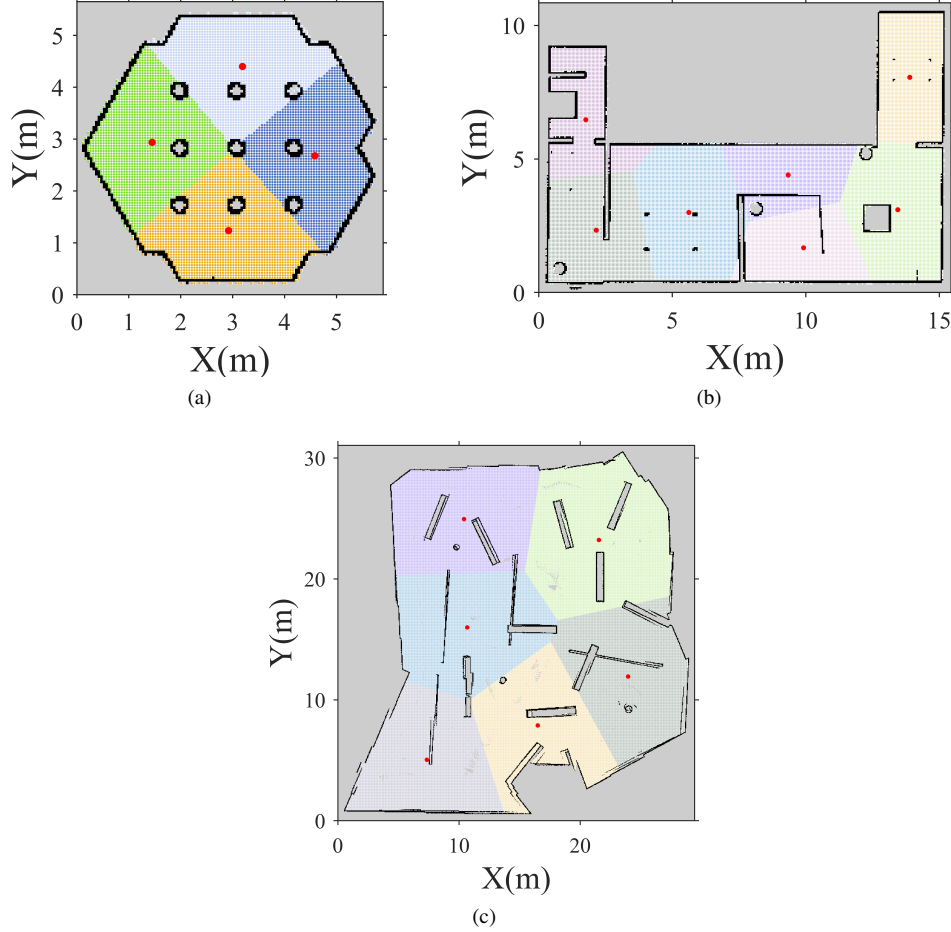


Figure 5: Map-zoning technique showcased on maps of environments of various sizes shapes and obstacle configurations. Each red dot indicates the centroid of a zone. All non-red dots which share the same color indicate a specific zone.

Algorithm 4 : *Logistician()*

- 1: **while** *Total Coverage rate* < *dc* **do**
 - 2: $|TF_{MS}, (X, Y)_{SM}, \text{sensor data}|_{at\ time\ t} \leftarrow$ ROS tf and sensor_msgs package
 - 3: *CoverageCalculator*($TF_{MS_t}, (X, Y)_{SM_t}, SR, SC_a, SC_{r_t}$)
 - 4: **end while**
-

3.3 Real-time computation technique for coverage calculation

This study has developed a real-time computation technique that utilizes descritized map data (via quadtree), sensor data, and matrix data structures for fast and accurate coverage rate calculation. The quadtree provides quick access (via querying) to all $Cell_F$ within the sensing range (SR) of the robot's sensor at a time t . All $Cell_F \in Query$ are then mapped onto sensor data received at t to match which $Cell_F \in Query$ is within the real sensor Field Of View (FOV) at time t . The coverage status of all $Cell_F \in Query$ which meet the matching are quickly stored to memory via matrices, and coverage is updated. All $Cell_F \in Query$ which do not meet this matching are dropped.

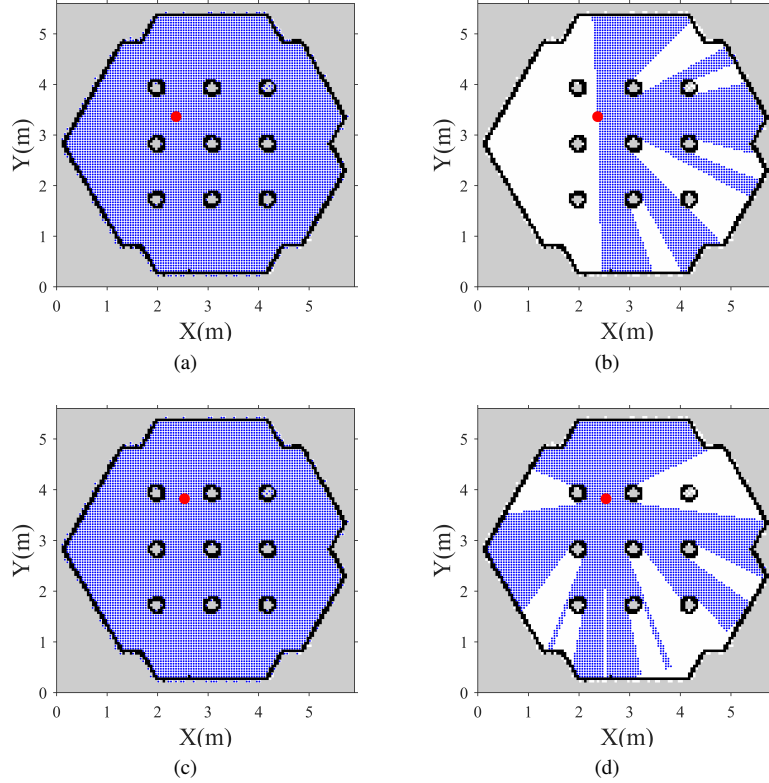


Figure 6: Mapping queried cells onto sensor data: (a) and (c) show all $Cell_F \in Query$. (b) and (d) show all $Cell_F \in Query$ that underwent successful sensor mapping with 2 different sensors. Red dot: sensor's position in the map frame $((X, Y)_{SM})$. Blue dots: all the $Cell_F \in Query$ before and after sensor mapping.

Figs. 6(a)-(d) illustrate the process. Figs. 6(a) and (c) show all $Cell_F \in Query$ (in blue). SR is 3.5m, and is converted to cell length by multiplication with res , so as to obtain the value of the querying radius as input for the quadtree algorithm. Figs. 6(a) and (b) correspond to a sensor with FOV ranging from -1.5 to 1.57 radians and Figs. 6(c) and (d) represent the results for a sensor with FOV ranging from 0 to 6.28 radians. To perform the sensor data mapping, every $(X, Y)_M$ derived from all $Cell_F \in Query$ must be transformed to coordinate points in the sensor frame using a TF_{MS} . This is so to get an accurate coverage from the FOV provided by the sensor. The *Logistician* function (Algorithm 4) continuously calls the *CoverageCalculator* function (Algorithm 5) to calculate coverage and publish the $(X, Y)_{zone}$ of least covered zones until dc is reached. The reason for this loop structure are as follows: (1) The relationship between the map frame and sensing frame (i.e., TF_{MS}) changes constantly as the robot moves around. Therefore, Algorithm 4 must continuously feed Algorithm 5 with new TF_{MS} information. (2) All the information provided by Algorithm 4 to 5 at each call must be time synchronized to get accurate coverage. That is to say that sensor data and the sensor position in the mapframe $((X, Y)_{SM})$ at the time t at which sensor data was received, are fed to Algorithm 5. TF_{MS} is time synchronized with this data as well. In this way Algorithm 5 and 6 are able to accurately recreate the FOV at a specific t . In subsection 3.3.1, all time synchronized data will be designated a subscript of t . The time interval between each call of Algorithm 5 is so minuscule that Algorithm 5 provides virtually continuous

coverage calculation even at robot speeds of 5m/s (to be discussed in section 4).

3.3.1 Algorithm flow

The *Logistician* function (Algorithm 4) receives TF_{MS_i} (published by the *tf* package) and sensor data (published by the *sensor_msgs* packages). The sensor data is published as a data field (*sensor_msgs/LaserScan.msg*, 2023).

$$\alpha = \text{int}(\tan \frac{Y_S}{X_S} \times \frac{180}{\pi}) \mod 360 \quad (8)$$

This data field contains the following information: (1) The array (SC_a) which contains the values of the scan angles of the sensor, and (2) the array (SC_{r_i}) which represents the scan range associated with each scan angle. It is important to not that the scan angles are converted from radians to degree values which are then rounded down to the nearest integer (just like the method seen in Eq. (8)). This enables the matching of orientations of cells to the scan angles. Algorithm 4 calls the *CoverageCalculator* function (Algorithm 5) which uses the sensor's position in the mapframe ($(X, Y)_{SM_i}$), TF_{MS_i} and SC_{r_i} as inputs. Algorithm 5 provides all $Cell_F \in \text{Query}$, TF_{MS_i} , and SC_{r_i} as inputs to the *Worker* function (Algorithm 6). The *Worker* function utilizes TF_{MS_i} , SC_a and SC_{r_i} to map each queried cell. A cell is successfully mapped by meeting two criteria: (1) First, the orientation (α ; calculated via Eq. (8)) is within the scan angles of the robot's sensor. α is the orientation of the point coordinate of the cell ($(X, Y)_S$) in the sensor frame. Then, on passing the first criteria, (2) the distance ($dist$) of the $(X, Y)_S$ of cell from the sensor is less than the scan range at the corresponding scan angle. All cells which successfully pass the two criteria are accounted to memory using the storage matrix M_C . The M_C matrix stores the coverage status and zone identification of every $Cell_F$ in the occupancy-grid map in order to make sure that: (1) covered cells aren't counted twice, and (2) the coverage of each cell counts towards the coverage of the zone it is assigned.

$$M_Z(zid, 4) = \frac{M_Z(zid, 3)}{M_Z(zid, 2)} \times (100) \quad (9)$$

$$\text{Total Coverage rate} = \frac{\sum_{n=0}^{n_z-1} M_Z(n, 3)}{(\text{number of } Cell_F \in \text{Occupancy} - \text{grid map})} \times 100 \quad (10)$$

Algorithm 5 : *CoverageCalculator*(TF_{MS} , $(X, Y)_{SM_i}$, SR , sc_a , sc_{r_i})

- 1: Query every $Cell_F$ within SR of $(X, Y)_{SM_i} \leftarrow$ Requires use of Eq. (6) and converting SR to from meters to cell length
 - 2: *Worker*($TF_{MS_i} \subseteq \text{all } Cell_F \in \text{Query}$, sc_a , sc_{r_i}) \leftarrow create threads of *Worker* function, each thread with approximately the same size of $\subseteq (\text{all } Cell_F \in \text{Query})$
 - 3: Find zones with the minimum $c_z \leftarrow M_Z(:, 4)$
 - 4: If there is more than one such zone, choose the zone of smallest d
 - 5: Share chosen zone's centroid information to *ATP*
 - 6: *Total Coverage rate* \leftarrow Eq. (10)
 - 7: **if** *Total Coverage rate* $\geq dc$ **then**
 - 8: *Stop*
 - 9: **end if**
-

Each row of M_C stores information about an individual $Cell$. The columns of M_C contain the following information from left to right: *ind* values of all cells in the occupancy-grid map, zone identifier (*zid*), coverage status. It should be noted that: (1) all $Cell_O$ and $Cell_U$ are not assigned any zone identifiers. (2) Every *zid* represents a row of M_Z . (3) The coverage status column keeps account of all $Cell_F$ which have been accounted for. Each cell has a column value of 0 when unaccounted, and a value of 1 when accounted. This column continuously updates itself as the program runs. Once a cell's coverage status is updated in M_C , c_z is also updated in storage matrix M_Z (see Eq. (9)). Algorithm 5 then uses the fourth column of M_Z to calculate the total coverage rate (*tc*) (see Eq. (10)). Algorithm 4 continuously

Algorithm 6 : $Worker(TF_{MS}, \subseteq allCell_F \in Query, sc_a, sc_{r_i})$

```
1: for  $Cell_F \in Query$  do
2:    $ind \leftarrow \text{Eq. (3)}$ 
3:   if  $M_C(ind, 2) == 0$  then
4:      $(X, Y)_M \text{ of } Cell_F \leftarrow \text{Eq. (4)}$ 
5:      $(X, Y)_S \text{ of } Cell_F \leftarrow \text{dotproduct}(TF_{MS}, (X, Y)_M)$ 
6:      $\alpha \leftarrow \text{Eq. (8)}$ 
7:     if  $\alpha \in SC_a$  then
8:        $dist \leftarrow \text{distance between sensor and } (X, Y)_S$ 
9:       if  $dist < sc_{r_i} \text{ at } \alpha$  then
10:         $M_C(ind, 2) = 1$ 
11:         $zid \leftarrow M_C(ind, 1)$ 
12:         $M_Z(zid, 3) + = 1$ 
13:         $M_Z(zid, 4) \leftarrow \text{Eq. (9)}$ 
14:      end if
15:    end if
16:  end if
17: end for
```

invokes Algorithm 5 in a loop until dc is reached, at which point Algorithm 5 communicates to Algorithm 4 and 1 to shut down. In this paper, Algorithm 5 includes a multithreading option that divides the cells $\in Query$ into subsets, which are then processed with separate threads of Algorithm 6 for possibly faster computation.

4 Experiments and Results

To validate the proposed methods described in this paper, three experiments have been conducted: (1) A comparison of *CT* performance of our CCPP application to the more established CPP method, boustrophedon coverage path planning (BCPP). These tests will be carried out in three simulated environments of varying size, shape, and obstacle density. The robot used in these tests was a Turtlebot3 with a 2D LiDAR (*FOV* ranging from 0 to 6.28 radians). (2) Live-testing in a classroom environment. The robot used in this test was a Turtlebot2 with a camera sensor (with a *FOV* ranging from -1.047 to 1.047 radians). A video of the trial is available ¹. (3) Test of computational speed of coverage calculation method. This experiment is carried out in a simulated environment. An additional experiment is also showcased at the end of this section to discuss the influence of parameters (specifically n_{iter} and the number of zones) on coverage time. The source code of our CCPP application is available ².

4.1 Comparing performance of CCPP and BCPP applications

BCPP (Choset, 2000; Choset and Pignon, 1998) is a fairly common method for CPP used in various applications, such as cleaning (Ntawumenyikizaba et al., 2012), agriculture (Coombes et al., 2019), demining (Bähnemann et al., 2021), multi-robot coverage (Rekleitis et al., 2008), and as such. The primary reasons for using BCPP for comparison are as follows. (1) Using a widely researched method in the field of CPP will provide a good benchmark for our method's performance. (2) There are open-source BCPP applications available for this comparison (ethz-asl / polygon_coverage_planning github, 2023; Rjxjp/coverageplanning github, 2023; nobleo/full_coverage_path_planner github, 2023; ipa320/ipa_coverage_planning github, 2023; irvingvasquez / ocpp github, 2023; Greenzie / boustrophedon_planner github, 2023; Ipiano / coverage-planner github, 2023), compared to other methods used in CPP, which are not publicly available to our knowledge. Boustrophedon planning is a method for generating a path for a robot that alternates back and forth across an area. This planning is usually paired with cell decomposition, a technique used to divide a 2D space into simple polygons (cells), and boustrophedon planning and cell decomposition are aptly named

¹Link to video

²https://gitlab.com/dsim-lab/paper-codes/Autonomous_search_of_real-life_environments

boustrophedon cellular decomposition. Each cell represents free space. The boustrophedon paths generated to cover each cell is guided by the shape of the obstacles and boundaries surrounding said cell. The boustrophedon cellular decomposition method, like this works method, is therefore an offline coverage path planning technique that requires prior knowledge of the size and shape of the environment and all obstacles within.

4.1.1 Comparing coverage times

To compare the performance of our CCPP method with that of BCPP, we used the BCPP application developed in ROS and provided in (ethz-asl / polygon_coverage_planning github, 2023) (the accompanying paper is (Bähnmann et al., 2021)). It was difficult to operate the other open-source applications, and technical support from the contributors to those applications was lacking. It must be noted that the BCPP application used in this paper provides coverage times based on more theoretical calculations, as the coverage path plan created was not tested in a Gazebo simulation like the CCPP application. To our knowledge, the coverage path planner provided by (ethz-asl / polygon_coverage_planning github, 2023) only provides a visual representation of the generated path. This means the BCPP application just shows what the path plan would look like based on the parameters. The coverage time is calculated based on the generated path and the parameters. The procedure to provide this path plan to the simulated robot (in gazebo) to enact it was not made clear to us. We consider three different environments shown in Fig. 7.

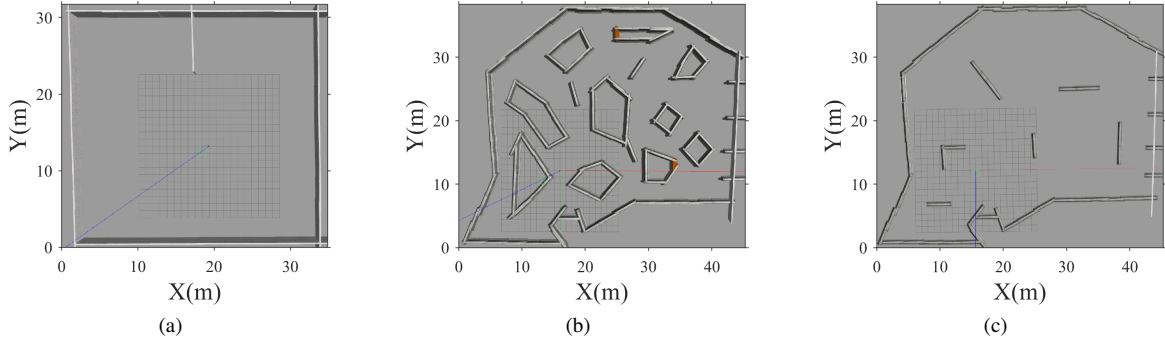


Figure 7: Simulated environments (a) Esquare, (b) Ldense, and (c) Hdense.

The environments are significantly larger than the robot's size, to provide large areas to cover. These environments vary in size, shape and obstacle density to provide a varied range of scenarios for analysis. Fig. 7(a) shows a simple-shaped environment with one wall obstacle, while Figs. 7(b)-(c) show complex-shaped environments with sparse and high obstacle density, respectively. The names of these environments are: (1) Esquare (fig. 7(a)), (2) Ldense (fig. 7(b)), and (3) Hdense (fig. 7(c)). To perform an accurate comparison, we have set the parameters for both applications to values that ensure that: (1) both applications achieve an estimate of 100% coverage rate (tc) for each environment. This aspect of the experiment is further discussed later. (2) Both applications adhere to the same physical constraints placed on the Turtlebot3. And (3) tc is achieved within a reasonable time frame. It is important to note occasional inaccuracies in map generation during SLAM, some of the obstacles are represented as containing free space. In other occasions, such free space could be created outside the walls of map representation of the environment. This free space would be non-existent in the real world. These inaccuracies occur as a result of bad sensor data. In turn, any $Cell_F$ within the non-existent free space could be covered as result of bad sensor data. For both the BCPP and CCPP applications, we set the robot's velocity to 0.22 m/s for all runs. To achieve coverage of all environments using BCPP, we set certain parameters (available in the configuration folder of the application) at constant values. These parameters are: (1) lateral overlap, which is set to 0 to maximize sweep distance and obtain the best possible coverage times, (2) maximum acceleration, set to 0.3 m/s² (the maximum acceleration of the Turtlebot3), and (3) wall distance, set to 0.2 m to account for the dimensions of the robot, which has a width of 0.173 m (its largest dimension). For the comparison, we varied the lateral footprint parameter for each environment. It is important to note that the lateral footprint parameter sets the sweep distance and is analogous to SR . The lateral footprint for Esquare, Ldense, and Hdense is 3.5 m, 2.0 m, and 1.5 m, respectively. The reason for the decrease in lateral footprint as map shape complexity and obstacle

density increase is to ensure thorough coverage. Fig. 8 shows the BCPP coverage for the different environments. Figs. 8(a)-(c) showcase the cell decompositions, and Figs. 8(d)-(f) showcase the robot's sweep across the environments. All the maps in Fig. 8 were manually created in the application and are therefore a close representation of the actual maps (generated via SLAM). Some of the obstacles and the boundary itself have been slightly simplified to enable computation of polygons. The "S" and "G" icons shown in green and red are the start and stop positions of the sweeps.

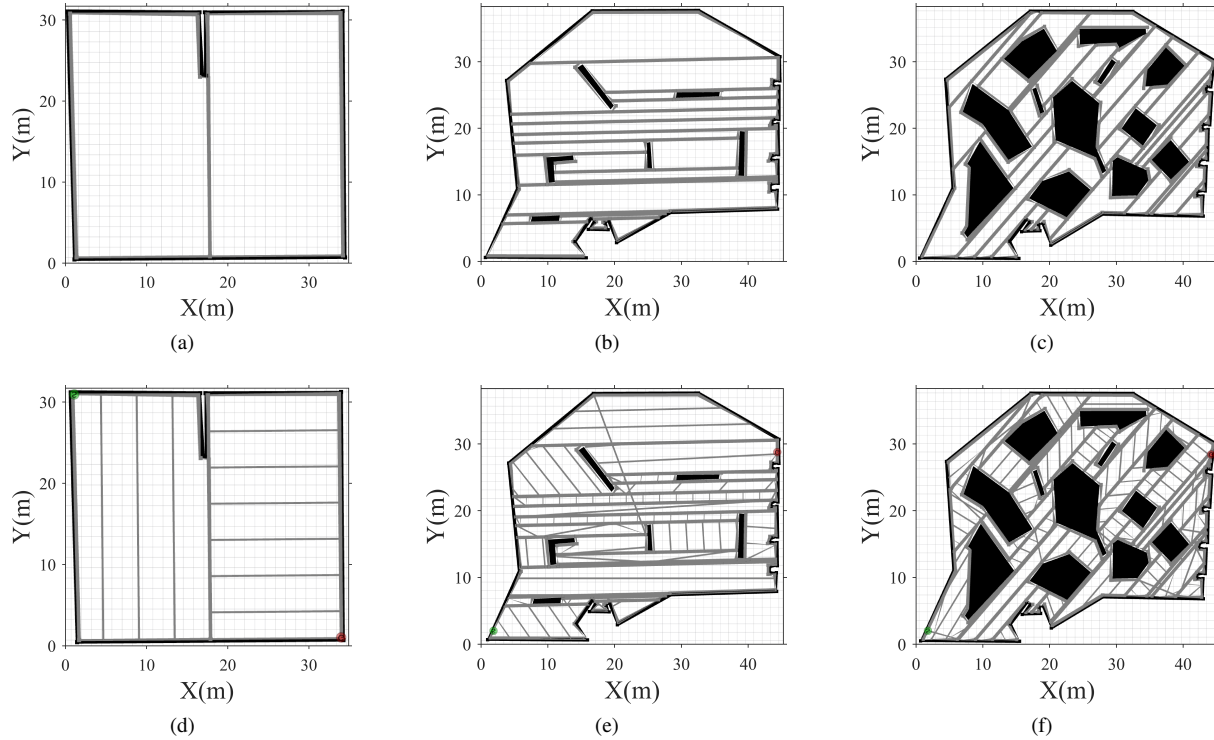


Figure 8: Coverage of simulated environments using BCPP: (a), (b) and (c) show the cellular decomposition of the maps of Esquare, Ldense and Hdense respectively. (d), (e) and (f) show the boustrophedon coverage path plan across the maps of Esquare, Ldense and Hdense respectively.

Fig. 9 show the coverage across these same environments using CCP. For CCP, the start position of the robot in each environment is kept the same as those used in the BCPP application for accuracy. The SR used for each map is the same as the lateral footprint values used. The parameter values of zones, n_{iter} , and n_s were chosen by trial and error. These parameters provided the smallest coverage times out of all the trials ran. Figs. 9(a)-(c) and 9(d)-(f) show the chaotic trajectories and covered cells for each environment, respectively. For the CCP application, the dc for every environment is set to 97% for the following reasons: (1) For the BCPP application, the tc is not outright provided as part of the output. It is difficult to visually discern how complete the coverage is. For more complex-shaped maps, the tc might not be 100% as a result of the simplified polygons used to describe the obstacles. This aspect of performance drop off of BCPP is further discussed in section 4.2. (2) To compensate for the previously discussed map inaccuracies during SLAM. As the algorithms account for non-existent free space in coverage calculations. (3) The CCP application shares the same difficulty in reaching a tc of 100% as chaotic trajectories cannot be fully controlled. Additionally, the SR values used to cover each map makes it more difficult to reach 100% tc with chaotic trajectories. This is especially true for the more complex-shaped maps.

As seen in Table 1, the BCPP provides faster coverage. At the parameters chosen, our CCP is approximately 2.3, 1.9, and 1.5 times slower than the BCPP application for Esquare, Ldense, and Hdense environments respectively. The BCPP process is more systematic in that (1) there is a prior knowledge of the dimensions and shapes of the boundaries

Table 1: Performance of BCCP and CCPP in various maps.

Map	Approximate free area (m^2)	SR /Lateral footprint (m)	n_{iter}	ns	zones	BCCP CT (min)	CCPP CT (min)	time ratio
Esquare	1010.44	3.5	20	20	40	17.08	39.28	2.30
Ldense	1217.47	2.0	20	20	60	54.09	101.08	1.89
Hdense	895.18	1.5	20	20	90	63.61	92.37	1.45

and obstacles of the environments which enables effective path tracing within cells. (2) The application uses a start and goal position to generate an overall coverage path plan which minimizes repeated coverage as the robot journeys from cell to cell, therefore optimizing CT . These attribute of BCCP result in the creation of a more absolute predetermined coverage path plan with very little wasted robot motion.

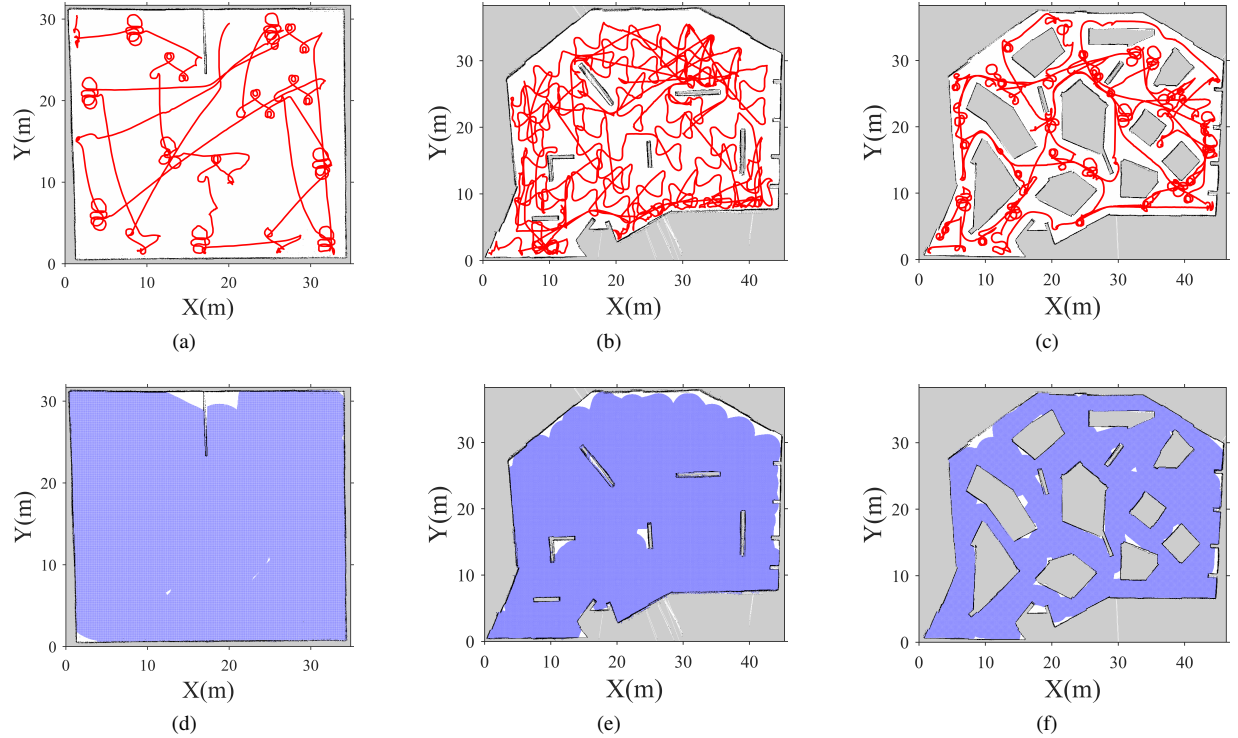


Figure 9: Coverage of simulated environments using CCPP: (a)-(c) show the chaotic trajectories across the maps of Esquare, Ldense and Hdense respectively. (d)-(f) show the 97% coverage (as a result of aforementioned trajectories) of the maps of Esquare, Ldense and Hdense respectively.

The CCPP is not as systematic for the reasons that: (1) CCPP corresponds to much less explicit planning and control of the trajectories compared to BCCP; the paths from start to the end of coverage are not predetermined but rather pseudo random. Other than the techniques we used to disperse the chaotic trajectories and the obstacle avoidance technique, this work does not use any other sort of planning for the trajectories. (2) It is perhaps possible that a different set of parameters not tried would have brought the coverage times closer to those of the BCCP application. Additionally, as discussed earlier, the BCCP application used in this paper provides a more theoretical coverage time. Additionally, CCPP ends at longer coverage times as the method must balance between two goals as opposed to just one, as unpredictable movement must be maintained while providing coverage. However, these times show the performance of CCPP and BCCP are reasonably comparable.

4.2 Potential advantages of CCPP over BCPP

When it comes to sensor based coverage applications, our CCPP method is more adaptable to various types of obstacles. The boustrophedon cellular decomposition method requires the setting of obstacles as polygons and as such. At the software level, the BCPP application is rendered unable to generate a path plan if the polygon shapes are too complex to generate based on the complex-shaped obstacles. This is a worst case scenario. On the other hand, if complex obstacle types are described as simpler polygon shapes to enable cellular decomposition, there runs the risk of less thorough coverage. Simpler polygon shapes (the cells created) can create areas to be covered which do not (perhaps to some significant degree) accurately represent the total area of free space in the actual physical environment and therefore this path plan strategy significantly drops off in terms of performance of coverage task. This issue may get compoundingly worse in sensor based surveillance task scenarios depending on the *FOV* of the sensor used in the real world. In order to mitigate performance issues, the *SR* of sensors (dependent on characteristics of the environment) may not be fully utilized. That is to say, a sweep distance (or in this case the lateral footprint parameter) much smaller than the *SR* might be used to ensure a more thorough coverage. The *CT* increases as a result. Fig. 10 showcases an example of potentially reduced BCPP performance. In Fig. 10, the lateral footprint as usual mimics the *SR* of the LiDAR. The BCPP application covers the Hdense environment with a lateral footprint of 3.5 m. The *CT* was 44.88 minutes. Though theoretically possible, it is visually unclear if there is any actual drop off in coverage performance with this lateral footprint value.

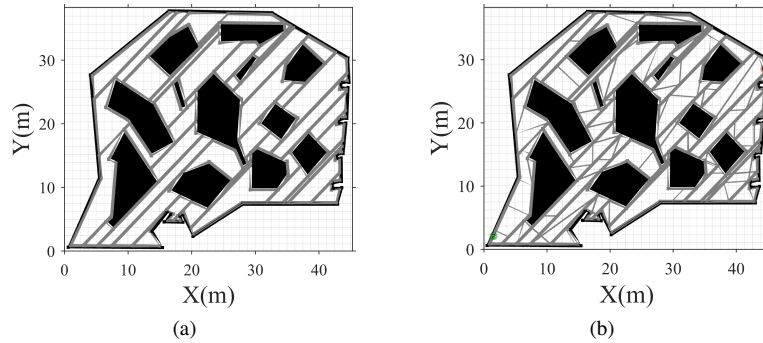


Figure 10: BCPP application used in Hdense using a lateral footprint of 3.5 m.

In order to mitigate any theoretical performance drop off, a user of this application may have to set the lateral footprint parameter at smaller values. However, simply reducing the lateral footprint does not ensure a more thorough coverage, as the shape and size of the cells may have already created a segments of free space that will not allow for better coverage of the physical environment. Our CCPP application does not have these drawbacks. Within the context of coverage path planning methodology, CCPP does not depend on polygon representation for the path planning process and therefore bypasses any hurdles involving computational complexity in this area. As long as our CCPP application is provided with an accurate occupancy-grid map, it can handle a wider variety of obstacle types and environments provided with an accurate occupancy-grid map, as well as provide absolute certainty that the desired coverage of the physical environment was met upon completion. For surveillance tasks, the performance of our CCPP application does not suffer as a result of *SR*, as it does not affect the path planning process by the same mechanism as with surveillance tasks. Fig. 11 showcases the performance of our CCPP in the Hdense environments at 97% coverage. The *SR* was 3.5 m and the *CT* was 44.24 minutes. Fig. 11 shows that our CCPP method provides comparable coverage times as the BCPP while providing possibly more accurate coverage. Section 4.2.1 will further discuss the performance problems that arise when BCPP faces worst case scenario computational complexity issues, and some additional problems thereof.

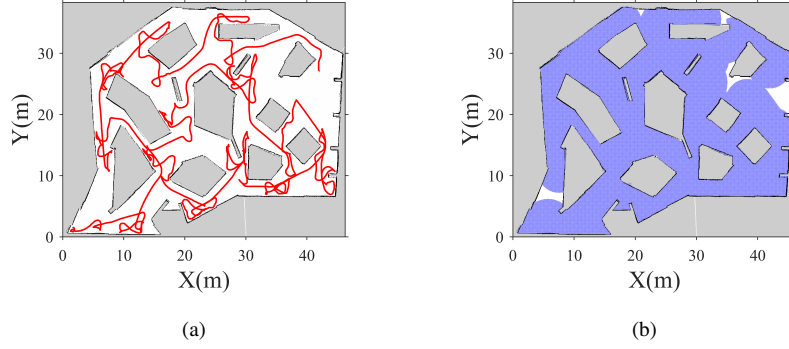


Figure 11: CCPP application used in Hdense using a SR of 3.5 m.

4.2.1 Coverage of a classroom with a Turtlebot2 with CCPP and BCPP applications

This section showcases the performance of our CCPP against BCPP in a real environment. The environment for this experiment was a classroom on campus (see Fig. 12). Some chairs were placed on tables to provide environmental variety and improve ease of map creation via SLAM. As in section 4.11, the parameters were set as follows: (1) n_{iter} was set to 20, (2) ns was set to 20, (3) the number of zones were set to 20 (4) v at 0.45 m/s, and (5) dc was set to 90%. The SR was 2.5 m. The camera sensor has a FOV of -1.57 to 1.57 radians. The coverage time at these parameters was 8.87 minutes. These parameters were arbitrarily chosen, and it is uncertain whether this coverage time is the shortest possible for this dc and SR .

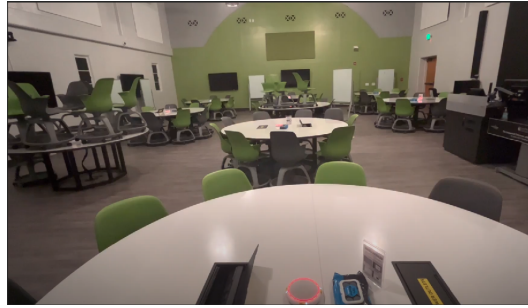


Figure 12: Picture of classroom used for live testing.

Fig. 13 represents the chaotic trajectories and coverage. The dc is set at 90% to compensate for the inaccuracies of the generated map. The SLAM process generated non-existent free space in certain areas of the map as result of sensor problems. This dc was a compromise to ensure the coverage task could be completed. The parameters of the BCPP application were set as follows. (1) The lateral footprint was set to 2.5 m, (2) the maximum acceleration was set to 0.1 m/s^2 (the maximum acceleration of the Turtlebot2), (3) the wall distance was set to 0.36 m to accommodate the size of the Turtlebot2. Fig. 14 showcases the cellular decomposition of the classroom with the BCPP application. As seen in Fig. 14, some of the obstacles (two sets of tables and chairs, and a white board) did not only have to be simplified, but combined into one polygon shape in order to ensure the cellular decomposition was computationally possible for the BCPP application to handle. Parts of the environment boundaries had to be simplified to this effect as well. The combination of sensor characteristics and inaccurate polygon representation could cause significant coverage performance drop off within the context of thoroughness of coverage. It is possible that our CCPP method has the same advantages across all methods which use cellular decomposition, such as the Morse-based cellular decomposition method (Galceran and Carreras, 2013).

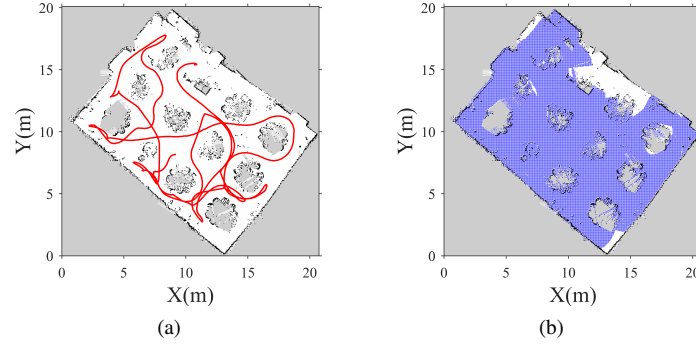


Figure 13: CCPP application used in a classroom for 90% coverage. The CCPP application provides the robot the ability to maneuver around the sets of tables and chairs, as well as the various whiteboards spread in the map.

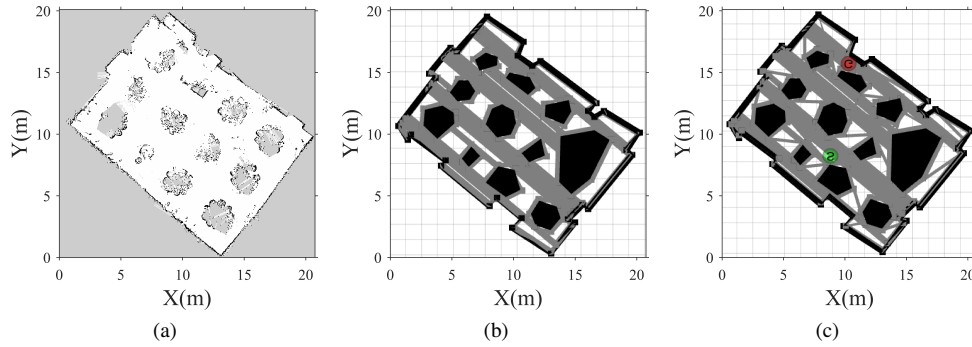


Figure 14: BCPP application used to cover classroom. A side by side view of the map in (a) (generated via SLAM) and the polygon representation of the environment (b-c) show the critical differences in environment representation.

4.3 Test of computational speed of coverage calculation technique

This experiment was developed to test the computational performance of our coverage calculation method. The setup for this experiment is as follows. (1) The maximum velocity of the simulated TurtleBot3 is set to 5m/s. (2) The robot's starting position is at one end of a runway. The robot is driven in a straight line to the opposite end of the runway, which ends at a wall. (3) Upon the robot's maximum velocity reaching 5m/s, the algorithms are signaled to start coverage calculation until the robot stops at the wall. (4) The distance traveled between each call of Algorithm 5 is recorded throughout the journey. Table 2 contains the maximum, minimum and average recorded distance of each experiment.

Table 2: Performance of computational speed of coverage calculation.

Runway	v (m/s)	SR (m)	Average distance (m)	Max distance (m)	Min distance (m)
Runway 1	5.0	5.0	2.29	3.16	1.84
Runway 2	5.0	7.5	5.84	11.00	3.66

These recorded distances provide the basis for judging the computational efficiency of coverage calculation. If the average recorded distance is less than the SR , this means that coverage updates occur at a faster rate than the robot is able to completely move out of the area covered during the previous call of Algorithm 5. For this experiment, the sensor FOV is set from 0 to 6.28 radians, and sensor FOV mapping is configured so that all queried cells are covered regardless of the outcome of success or failure of their mapping to sensor data. This configuration was set so as to maximize the computational burden placed on our coverage calculation method, specifically the *CoverageCalculator*

function which is responsible for updating zone coverage and cell coverage status (with M_Z and M_C respectively). In this way, accurate coverage is neglected for the sake of these experiments. We did not use the multi-threading option to this effect as well. A maximum velocity of 5m/s was the highest that the simulation would allow without creating computational errors within the physics engine of Gazebo.

Fig. 15 depicts the trajectory of the Turtlebot3 and it's coverage across the two different runways used for this experiment. The smallest runway (Figs. 15(a) and (b)) is covered using an SR of 5.0m. The average, maximum and minimum recorded distances are 2.29m, 3.16m, and 1.84m, respectively. This means that at no point is there a gap in coverage update, that is to say, from the first to the last call of Algorithm 5, the entire area within that time frame is covered (as seen in Fig. 15(b)). The biggest runway (Figs. 15(c) and (d)) is covered using an SR of 7.5m. The average, maximum and minimum recorded distances are 5.84m, 11.0m, and 3.66m, respectively. The average distance suggests that most of the area between the time of the first and last call is covered. The maximum distance shows that there will be gaps in coverage, which Fig. 15(d) depicts as such. Because these experimental results show coverage as a robot moves solely in a straight line, they must therefore be taken as a sort of worst-case-scenario. Most of the area at the wider segment of the largest runway is still covered. This section shows that the computation speed of coverage calculation enables effective coverage rate update even at robot speeds of up to 5m/s with SR at 7.5m. The high speed of coverage calculations ensures computationally efficient coverage for our specific application.

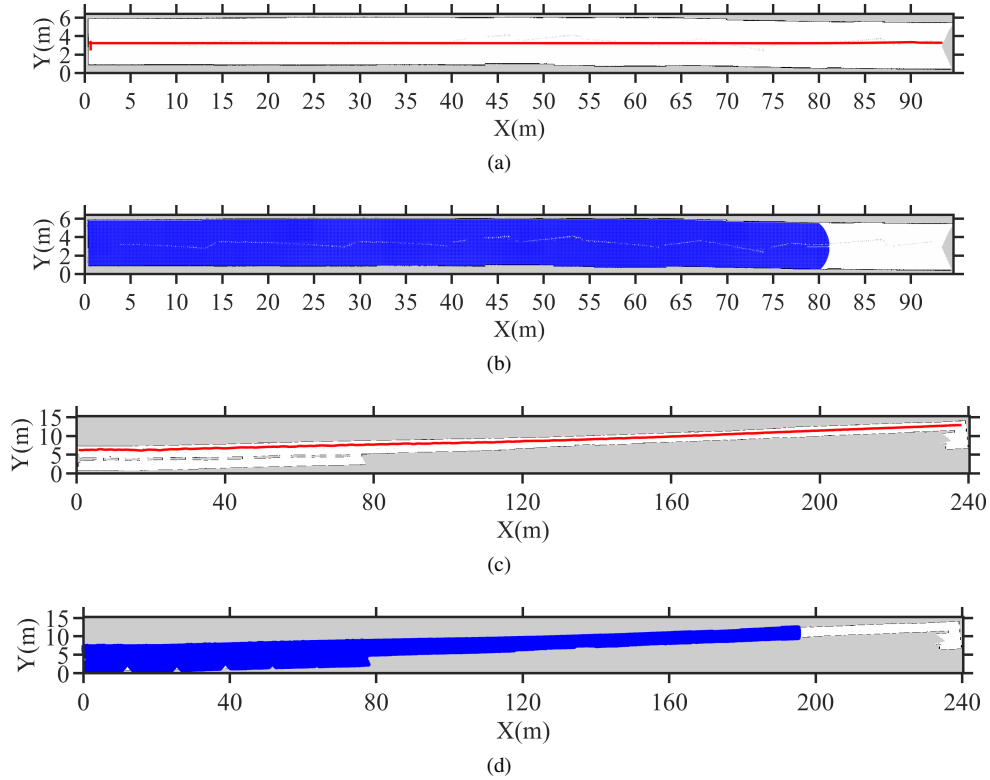


Figure 15: The performance of the coverage calculation method is tested using 2 runways. The figures depict: (a) The straight line trajectory of robot from one end of the smallest runway to the other. (b) The coverage started from the point at which simulated Turtlebot3 reaches a maximum velocity of 5m/s on aforementioned trajectory. (c) The straight line trajectory of robot from one end of the largest runway to the other. (d) The coverage started from the point at which simulated Turtlebot3 reaches a maximum velocity of 5m/s on aforementioned trajectory.

4.4 Parameters influence and Future Directions

This section discusses the effect of parameters on coverage time. Various environments have been covered multiple times using different sets of parameters, and the resulting coverage times have been recorded in Table 3. Fig. 16

depicts the maps of these environments. The names of the environments shown in Figs. 16(a)-(b) are: (1) Bungalow, and (2) LDW1 in that order. The dc for every experiment was set to 90%. The robot's starting position was kept the same for every test carried out in an environment, and the v for every experiment was 0.22m/s. The FOV for all experiments is 0 to 6.28 radians. The SR for all experiments is 3.5m. The results in Table 3 show general patterns in coverage performance within the context of CT . With all other parameters constant, CT increases as n_{iter} increases (see case 1 and 3, case 5 and 6). This makes sense due to the unpredictability of motion at a high n_{iter} might increase likelihood of repetitive coverage. There is also the added factor that: (1) the number of zones increases the probability of the spread of chaotic trajectories to unexplored areas in the environment, (2) the total area of free space in these two simulated environments is small relative to the maximum sensing area of the robot. As a result, it is more effective to set n_{iter} to lower values so the robot does not spend as much time repetitively moving around any one local area and can more effectively traverse to least covered areas. As an example, the area of free space of LDW1 is $1146.34m^2$, and the maximum sensing area given the FOV and SR is $38.48m^2$. The number of zones used in case 8 and 11 is 25. This brings the average size of a zone to $45.85m^2$. Simply moving to the centroid of a new zone could cover a substantial amount of it. It is therefore reasonable to reduce the n_{iter} from 1000 (case 6) to 20 (case 5) to reduce the amount of repetitive coverage. In the scenario where the sensing area is comparable to the average size of a zone, a further increase in the number of zones may provide negligible effect to CT (see case 1 and 2). At this point the value of n_{iter} can be set very low and achieve quick coverage, as in case 4. Setting the n_{iter} very low will for the sake of a much shorter CT greatly sacrifices the unpredictability of motion, which is one of the main draws to use a CCPP application in the first place. Future studies must focus on the development of a method (perhaps a deep-learning model) which optimizes these aforementioned parameters (as well as others such as dt) based on the total free area of the environment, FOV , SR and v . In this way, some sort of decision making strategy can be implemented which can dependably choose parameters that balance unpredictability of trajectories with CT performance, favoring one over the other based on task objectives.

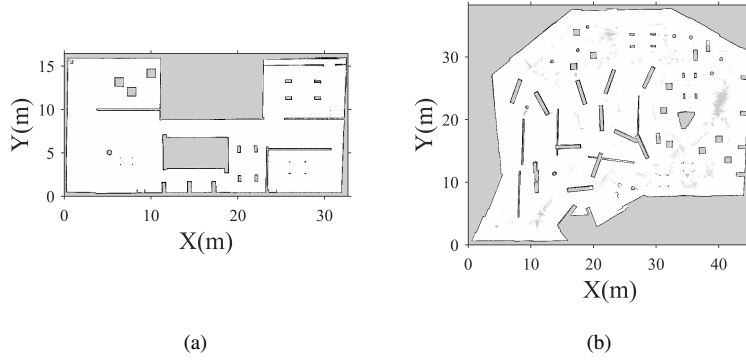


Figure 16: Maps of simulated environments: (a) Bungalow, and (b) LDW1.

Table 3: Performance of CCPP on two environments under various parameters.

Map	Approximate free area(m^2)	set	SR (m)	n_{iter}	ns	zones	CT (min)
Bungalow	365.03	1	3.50	40	20	50	29.00
		2	3.50	40	20	100	34.00
		3	3.50	1000	20	50	115.00
LDW1	1146.34	4	3.50	10	10	25	26.21
		5	3.50	20	20	25	54.00
		6	3.50	1000	20	25	241.00

5 Conclusions

This study proposes new techniques to realize the application of CCPP in realistic environments. Three techniques were developed to achieve this goal. The developed coverage calculation technique was shown to be computationally efficient at speeds up to 5 m/s, while the robot's sensor has an SR of 7.5 m. These contributions were integrated to develop a new CCPP application in the ROS framework that enables effective coverage of large, complex-shaped environments with varying obstacle densities. Due to use of occupancy-grid maps, our method is susceptible to exponential memory usage dependent on size of environment and resolution used for grid map representation. This could lead to memory errors. Further work must be done to tackle this issue. The performance of our CCPP application was tested against a more established CPP, the boustrophedon coverage path planner. The BCPP application used for this comparison performed coverage at shorter coverage times, but the CCPP was shown to have the potential to match it if provided with the right set of system parameters while providing the unpredictability of motion necessary to avoid attacks in adversarial environments. Further research is required to develop a machine-learning technique that enables CCPP to determine a proper combination of parameter values that would provide effective coverage based on the robot's properties and the known properties of the covered environment. The CCPP method was shown to have potential advantages over BCPP due to the computational complexity involved in cellular decomposition. It is therefore plausible that our CCPP method has these same advantages over all methods which use cellular decomposition, for instance, the Morse-based cellular decomposition method. Future study should involve the testing of our CCPP method against other types of CPP methods.

References

- Agiza, H. and Yassen, M. (2001). Synchronization of rossler and chen chaotic dynamical systems using active control. *Physics Letters A*, 278(4):191–197.
- Arrowsmith, D. K., Cartwright, J. H., Lansbury, A. N., and Place, C. M. (1993). The bogdanov map: Bifurcations, mode locking, and chaos in a dissipative system. *International Journal of Bifurcation and Chaos*, 3(04):803–842.
- Bae, Y. (2004a). Obstacle avoidance method in the chaotic robot. In *The 23rd Digital Avionics Systems Conference (IEEE Cat. No. 04CH37576)*, volume 2, pages 12–D. IEEE.
- Bae, Y. (2004b). Target searching method in the chaotic mobile robot. In *The 23rd Digital Avionics Systems Conference (IEEE Cat. No. 04CH37576)*, volume 2, pages 12–D. IEEE.
- Bae, Y., Lee, M., and Gatton, T. M. (2006). An obstacle avoidance method for chaotic robots using angular degree limitations. In *International Conference on Computational Science and Its Applications*, pages 244–250. Springer.
- Bae, Y.-C., Kim, J.-W., and Kim, Y.-G. (2003). Obstacle avoidance methods in the chaotic mobile robot with integrated some chaos equation. *International Journal of Fuzzy Logic and Intelligent Systems*, 3(2):206–214.
- Bähnemann, R., Lawrance, N., Chung, J. J., Pantic, M., Siegwart, R., and Nieto, J. (2021). Revisiting boustrophedon coverage path planning as a generalized traveling salesman problem. In *Field and Service Robotics: Results of the 12th International Conference*, pages 277–290. Springer.
- Choi, S., Lee, S., Viet, H. H., and Chung, T. (2017). B-theta*: an efficient online coverage algorithm for autonomous cleaning robots. *Journal of Intelligent & Robotic Systems*, 87(2):265–290.
- Choi, Y., Choi, Y., Briceno, S., and Mavris, D. N. (2020). Energy-constrained multi-uav coverage path planning for an aerial imagery mission using column generation. *Journal of Intelligent & Robotic Systems*, 97(1):125–139.
- Choset, H. (2000). Coverage of known spaces: The boustrophedon cellular decomposition. *Autonomous Robots*, 9:247–253.
- Choset, H. and Pignon, P. (1998). Coverage path planning: The boustrophedon cellular decomposition. In *Field and service robotics*, pages 203–209. Springer.

- Chu, H., Yi, J., and Yang, F. (2022). Chaos particle swarm optimization enhancement algorithm for uav safe path planning. *Applied Sciences*, 12(18):8977.
- Coombes, M., Chen, W.-H., and Liu, C. (2019). Flight testing boustrophedon coverage path planning for fixed wing uavs in wind. In *2019 International Conference on Robotics and Automation (ICRA)*, pages 711–717. IEEE.
- Curiac, D.-I. and Volosencu, C. (2014). A 2d chaotic path planning for mobile robots accomplishing boundary surveillance missions in adversarial conditions. *Communications in Nonlinear Science and Numerical Simulation*, 19(10):3617–3627.
- Di Franco, C. and Buttazzo, G. (2016). Coverage path planning for uavs photogrammetry with energy and resolution constraints. *Journal of Intelligent & Robotic Systems*, 83(3):445–462.
- ethz-asl / polygon_coverage_planning github (2023). https://github.com/ethz-asl/polygon_coverage_planning.
- Faigl, J., Kulich, M., and Přeučil, L. (2011). A sensor placement algorithm for a mobile robot inspection planning. *Journal of Intelligent & Robotic Systems*, 62(3):329–353.
- Fallahi, K. and Leung, H. (2010). A cooperative mobile robot task assignment and coverage planning based on chaos synchronization. *International Journal of Bifurcation and Chaos*, 20(01):161–176.
- Galceran, E. and Carreras, M. (2013). A survey on coverage path planning for robotics. *Robotics and Autonomous systems*, 61(12):1258–1276.
- Greenzie / boustrophedon_planner github (2023). https://github.com/Greenzie/boustrophedon_planner.
- Grøtli, E. I. and Johansen, T. A. (2012). Path planning for uavs under communication constraints using splat! and milp. *Journal of Intelligent & Robotic Systems*, 65(1):265–282.
- Hameed, I. A. (2014). Intelligent coverage path planning for agricultural robots and autonomous machines on three-dimensional terrain. *Journal of Intelligent & Robotic Systems*, 74(3):965–983.
- Hsu, P.-M., Lin, C.-L., and Yang, M.-Y. (2014). On the complete coverage path planning for mobile robots. *Journal of Intelligent & Robotic Systems*, 74(3):945–963.
- Huang, X., Sun, M., Zhou, H., and Liu, S. (2020). A multi-robot coverage path planning algorithm for the environment with multiple land cover types. *IEEE Access*, 8:198101–198117.
- ipa320/ipa_coverage_planning github (2023). https://github.com/ipa320/ipa_coverage_planning.
- Ipiano / coverage-planner github (2023). <https://github.com/Ipiano/coverage-planning>.
- irvingvasquez / ocpp github (2023). <https://github.com/irvingvasquez/ocpp>.
- Jan, G. E., Luo, C., Lin, H.-T., and Fung, K. (2019). Complete area coverage path-planning with arbitrary shape obstacles. *Journal of Automation and Control Engineering Vol*, 7(2).
- Jansri, A., Klomkarn, K., and Sooraksa, P. (2004). On comparison of attractors for chaotic mobile robots. In *30th Annual Conference of IEEE Industrial Electronics Society, 2004. IECON 2004*, volume 3, pages 2536–2541. IEEE.
- Kapoutsis, A. C., Chatzichristofis, S. A., and Kosmatopoulos, E. B. (2017). Darp: divide areas algorithm for optimal multi-robot coverage path planning. *Journal of Intelligent & Robotic Systems*, 86(3):663–680.
- Li, C., Song, Y., Wang, F., Liang, Z., and Zhu, B. (2015). Chaotic path planner of autonomous mobile robots based on the standard map for surveillance missions. *Mathematical Problems in Engineering*, 2015.
- Li, C., Song, Y., Wang, F., Wang, Z., and Li, Y. (2016). A bounded strategy of the mobile robot coverage path planning based on lorenz chaotic system. *International journal of advanced robotic systems*, 13(3):107.
- Li, C., Wang, F., Zhao, L., Li, Y., and Song, Y. (2013). An improved chaotic motion path planner for autonomous mobile robots based on a logistic map. *International Journal of Advanced Robotic Systems*, 10(6):273.

- Li, C.-h., Song, Y., Wang, F.-y., Wang, Z.-q., and Li, Y.-b. (2017). A chaotic coverage path planner for the mobile robot based on the chebyshev map for special missions. *Frontiers of Information Technology & Electronic Engineering*, 18(9):1305–1319.
- Li, Y., Li, D., Maple, C., Yue, Y., and Oyekan, J. (2014). K-order surrounding roadmaps path planner for robot path planning. *Journal of Intelligent & Robotic Systems*, 75(3):493–516.
- Lü, J., Chen, G., and Cheng, D. (2004). A new chaotic system and beyond: the generalized lorenz-like system. *International Journal of Bifurcation and Chaos*, 14(05):1507–1537.
- Majeed, A. I. (2020). Mobile robot motion control based on chaotic trajectory generation. *Journal of Engineering and Sustainable Development*, 24(4):48–55.
- Moysis, L., Petavratzis, E., Marwan, M., Volos, C., Nistazakis, H., and Ahmad, S. (2020a). Analysis, synchronization, and robotic application of a modified hyperjerk chaotic system. *Complexity*, 2020.
- Moysis, L., Petavratzis, E., Volos, C., Nistazakis, H., and Stouboulos, I. (2020b). A chaotic path planning generator based on logistic map and modulo tactics. *Robotics and Autonomous Systems*, 124:103377.
- Moysis, L., Rajagopal, K., Tutueva, A. V., Volos, C., Teka, B., and Butusov, D. N. (2021). Chaotic path planning for 3d area coverage using a pseudo-random bit generator from a 1d chaotic map. *Mathematics*, 9(15):1821.
- Nakamura, Y. and Sekiguchi, A. (2001). The chaotic mobile robot. *IEEE Transactions on Robotics and Automation*, 17(6):898–904.
- Nasr, S., Mekki, H., and Bouallegue, K. (2019). A multi-scroll chaotic system for a higher coverage path planning of a mobile robot using flatness controller. *Chaos, Solitons & Fractals*, 118:366–375.
- nav_msgs/Path.msg (2023). http://docs.ros.org/en/api/nav_msgs/html/msg/Path.html.
- nobleo/full_coverage_path_planner github (2023). https://github.com/nobleo/full_coverage_path_planner.
- Ntawumenyikizaba, A., Viet, H. H., and Chung, T. (2012). An online complete coverage algorithm for cleaning robots based on boustrophedon motions and a* search. In *2012 8th International Conference on Information Science and Digital Content Technology (ICIDT2012)*, volume 2, pages 401–405. IEEE.
- Nwachima, C. and Pérez-Cruz, J. H. (2021). Analysis of a new chaotic system, electronic realization and use in navigation of differential drive mobile robot. *Chaos, Solitons & Fractals*, 144:110684.
- Petavratzis, E., Moysis, L., Volos, C., Gupta, M. K., Stouboulos, I., and Goudos, S. (2020a). Chaotic motion control of a mobile robot using a memory technique. In *2020 24th International Conference on System Theory, Control and Computing (ICSTCC)*, pages 506–511. IEEE.
- Petavratzis, E., Moysis, L., Volos, C., Nistazakis, H., Munoz-Pacheco, J. M., and Stouboulos, I. (2020b). Motion control of a mobile robot based on a chaotic iterative map. In *2020 9th International Conference on Modern Circuits and Systems Technologies (MOCAST)*, pages 1–4. IEEE.
- Petavratzis, E., Moysis, L., Volos, C., Nistazakis, H., Stouboulos, I., et al. (2020c). Chaotic path planning for grid coverage using a modified logistic-map map. *Journal of Automation, Mobile Robotics and Intelligent Systems*, pages 3–9.
- Petavratzis, E., Moysis, L., Volos, C., Stouboulos, I., Nistazakis, H., and Valavanis, K. (2021a). A chaotic path planning generator enhanced by a memory technique. *Robotics and Autonomous Systems*, 143:103826.
- Petavratzis, E., Volos, C., Ouannas, A., Nistazakis, H., Valavanis, K., and Stouboulos, I. (2021b). A 2d discrete chaotic memristive map and its application in robot's path planning. In *2021 10th International Conference on Modern Circuits and Systems Technologies (MOCAST)*, pages 1–4. IEEE.
- Pimentel-Romero, C., Muñoz-Pacheco, J. M., Felix-Beltran, O., Gomez-Pavon, L., and Volos, C. K. (2017). Chaotic planning paths generators by using performance surfaces. In *Fractional Order Control and Synchronization of Chaotic Systems*, pages 805–832. Springer.

- Quadtree implementation in Python (2020). <https://scipython.com/blog/quadtrees-2-implementation-in-python>.
- Rekleitis, I., New, A. P., Rankin, E. S., and Choset, H. (2008). Efficient boustrophedon multi-robot coverage: an algorithmic approach. *Annals of Mathematics and Artificial Intelligence*, 52:109–142.
- Rjixp/coverageplanning github (2023). <https://github.com/RJixp/CoveragePlanning>.
- Samet, H. (1988). An overview of quadrees, octrees, and related hierarchical data structures. *Theoretical Foundations of Computer Graphics and CAD*, pages 51–68.
- sensor_msgs/LaserScan.msg (2023). http://docs.ros.org/en/melodic/api/sensor_msgs/html/msg/LaserScan.html.
- Sooraska, P. and Klomkarn, K. (2010). "no-cpu" chaotic robots: from classroom to commerce. *IEEE circuits and systems magazine*, 10(1):46–53.
- Sridharan, K. and Ahmadabadi, Z. N. (2020). A multi-system chaotic path planner for fast and unpredictable online coverage of terrains. *IEEE Robotics and Automation Letters*, 5(4):5268–5275.
- Sridharan, K., McNamee, P., Nili Ahmadabadi, Z., and Hudack, J. (2022). Online search of unknown terrains using a dynamical system-based path planning approach. *Journal of Intelligent & Robotic Systems*, 106(1):1–19.
- Tlelo-Cuautle, E., Ramos-López, H. C., Sánchez-Sánchez, M., Pano-Azucena, A. D., Sánchez-Gaspariano, L. A., Núñez-Pérez, J. C., and Camas-Anzueto, J. L. (2014). Application of a chaotic oscillator in an autonomous mobile robot. *Journal of Electrical Engineering*, 65(3):157.
- Volos, C. K., Bardis, N., Kyprianidis, I. M., and Stouboulos, I. N. (2012a). Implementation of mobile robot by using double-scroll chaotic attractors. *Recent Researches in Applications of Electrical and Computer Engineering*, pages 119–124.
- Volos, C. K., Kyprianidis, I. M., and Stouboulos, I. N. (2012b). A chaotic path planning generator for autonomous mobile robots. *Robotics and Autonomous Systems*, 60(4):651–656.
- Volos, C. K., Kyprianidis, I. M., and Stouboulos, I. N. (2013). Experimental investigation on coverage performance of a chaotic autonomous mobile robot. *Robotics and Autonomous Systems*, 61(12):1314–1322.
- Zhang, C. (2018). Path planning for robot based on chaotic artificial potential field method. In *IOP Conference Series: Materials Science and Engineering*, volume 317, page 012056. IOP Publishing.
- Zhu, D., Tian, C., Sun, B., and Luo, C. (2019). Complete coverage path planning of autonomous underwater vehicle based on gbnn algorithm. *Journal of Intelligent & Robotic Systems*, 94(1):237–249.